Chemical looping dry reforming of methane using mixed oxides of iron and cerium: Operation window

Catalysis Communications 160 (2021) 106356

Contents lists available at ScienceDirect

Catalysis Communications

journal homepage: www.elsevier.com/locate/catcom

Short communication

Chemical looping dry reforming of methane using mixed oxides of iron and cerium: Operation window

F.R. García-García [a,*], I.S. Metcalfe [b]

[a] School of Engineering, Institute of Materials and Processes, University of Edinburgh, Robert Stevenson Road, Edinburgh EH9 3FB, UK
[b] School of Chemical Engineering and Advanced Materials, Newcastle University, Merz Court, Newcastle upon Tyne NE1 7RU, UK

ARTICLE INFO

Keywords:
Chemical looping reforming
Hydrogen production
Syngas production
Mixed oxides of iron and cerium

ABSTRACT

A series of the mixed oxides of iron and cerium, with an iron(III) oxide content ranging from 0 wt% to 100 wt% were tested as oxygen carriers in the chemical looping dry reforming of methane (CL-DRM). The reactivity during the CL-DRM significantly increased when iron and cerium are forming a mixed oxide. By careful control of the Fe_2O_3/CeO_2 mass ratio, initial oxidation state and reaction time the activity of the oxygen carrier material can be adjusted so as to substantially favour oxidation of methane to syngas and discourage both total oxidation of methane and carbon deposition *via* decomposition of methane.

1. Introduction

Chemical looping dry reforming of methane (CL-DRM) is a potential alternative to traditional steam reforming process, which can produce during the reduction step syngas with a $[H_2]/[CO]$ ratio equal to 2 [1]. Here, the lattice oxygen of a solid metal oxide (*i.e.* iron oxide) is used to oxidise partially the methane to hydrogen and carbon monoxide. The regeneration of the reduced metal oxide can be performed in a subsequent step by oxidation with carbon dioxide producing additional carbon monoxide. The CL-DRM is from an environmental point of view, since two greenhouse gas molecules (methane and carbon dioxide) are converted into valuable products (hydrogen and carbon monoxide).

The main challenge of CL-DRM using iron oxide as an oxygen carrier is to control the product selectivity to avoid both the complete oxidation of methane [2–4] and the deposition of carbon on the carrier [5]. Furthermore, iron oxides undergo significant chemical, thermal and physical stresses as oxides cycle between the fully-oxidised and fully-reduced condition, limiting their longevity. In this respect, it is well known that mixing iron oxides with different refractory oxides such as ceria, alumina, silica, titania and zirconia improves its resistance to sintering at high temperatures.

Among the different iron-based oxygen carriers, mixed oxides of iron and cerium appear to be attractive for chemical looping reforming processes, owing to their high capacity for storing oxygen and to the unique redox properties of cerium. The present research explores the behaviour of mixtures of iron and cerium oxides during the reduction step of the CL-DRM. The hypothesis examined was that reactivity and product selectivity can be enhanced by careful control of the starting oxidation state and composition of the oxygen carrier material. Whereas minimisation of coke formation can be achieved by limiting the duration of the reduction step of the CL-DRM.

2. Experimental

2.1. Preparation of the mixed oxides of iron and cerium

A series of mixed oxides of iron and cerium, with an iron(III) oxide content ranging from 0 wt% to 100 wt%, was prepared using the sol–gel Pechini method [6]. The dry gels were calcined in air in a tubular furnace (Lenton) at 900 °C for 1 h. After calcination, the mixed oxide powders were pelletised by applying a load of 10 t in a 13 mm diameter cylinder for 5 min. These pellets were then crushed and sieved to sizes ranging from 425 μm to 710 μm. The different mixed oxides of iron and cerium were labelled as follows; 100-C, 20-FC, 40-FC, 60-FC, 80-FC and 100-F corresponding to 0 wt%, 20 wt%, 40 wt%, 60 wt%, 80 wt% and 100 wt% iron(III) oxide, balance cerium(IV) oxide.

2.2. Characterisation of the mixed oxides of iron and cerium

The specific surface area and the pore volume of the fresh materials were determined from nitrogen adsorption isotherms at −196 °C (TriStar 3000 volumetric system). Prior to nitrogen adsorption, the

* Corresponding author.
E-mail address: francisco.garcia-garcia@ed.ac.uk (F.R. García-García).

https://doi.org/10.1016/j.catcom.2021.106356
Received 16 August 2021; Received in revised form 11 September 2021; Accepted 17 September 2021
Available online 20 September 2021

Table 1
Yields and selectivity during the reduction step of the CLR process for mixed oxides of iron and cerium after 90 min activation in carbon dioxide at 900 °C.

Materials	$H_{2\ (a)}$*	$H_{2\ (DM)}$**	CO	H_2O	Coke	$[H_{2\ (a)}$*$]/[CO]$	$[H_{2\ (b)}$***$]/[CO]$
	(mol)						
100-C	0.0013	0.0007	0.0002	0.0000	0.0003	1.7	1.7
20-FC	0.0072	0.0026	0.0017	0.0018	0.0013	1.5	2.8
40-FC	0.0066	0.0031	0.0006	0.0005	0.0015	1.8	2.2
60-FC	0.0074	0.0008	0.0000	0.0029	0.0004	2.0	9.9
80-FC	0.0083	0.0007	0.0000	0.0033	0.0003	2.0	11.6
100-F	0.0006	0.0001	0.0000	0.0001	0.0000	2.0	4.0

* Hydrogen produced during the partial oxidation of methane.
** Hydrogen produced by decomposition of methane (DM).
*** Total hydrogen produced (partial oxidation of methane + decomposition of methane).

oxides were degassed in argon at 150 °C overnight. The BET and BJH methods were used to obtain the specific surface area and the pore size and pore volume distributions, respectively.

The morphology and structure of the different mixed oxides of iron and cerium were studied using a scanning electron microscope (Carl Zeiss SIGMA HD VP Field Emission) equipped with an energy dispersive X-ray spectroscopy detector (EDX Oxford AZtec) which permit elemental analysis. The microscope operated under the following conditions: accelerating voltage 20 kV, current 8–10 nA, working distance 14 nm, vacuum in the chamber 10–270 Pa.

X-ray diffraction measurements were performed with a Bruker AXS D8 ADVANCE diffractometer with CoKα1 source ($\lambda = 0.1789$) in a wide-angle range (from 30° to 90° in 2θ). The lattice constant of iron and cerium crystals was calculated by Rietveld refinement.

Hydrogen temperature programmed reduction (H_2-TPR) was performed on a Micromeritics Autochem-II instrument equipped with a TCD detector. The samples (30 mg) were previously dried in argon flow at 120 °C switched to 50 mL/min (STP) of 5 vol% hydrogen in argon. The temperature was raised from room temperature to 900 °C at 10 °C/min.

2.3. Performance of the mixed oxides of iron and cerium

The performance of mixed oxides of iron and cerium during different chemical looping reforming (CLR) experiments was determined in a fixed-bed reactor at 1 atm and 900 °C using 500 mg of material. A typical CLR experiment involved 10 redox cycles. In each cycle, the material was exposed to the following gaseous environments in turn: i) 1 min purge in nitrogen, ii) 90 min activation in buffer gas (*i.e.* air, carbon dioxide or hydrogen), iii) 1 min purge in nitrogen and iv) 10 min reduction in 10 vol% methane. In all experiments, the feed gas flow rate was constant and equal to 1.5 L/min (STP). The composition of the exit gases (methane, hydrogen, carbon monoxide and carbon dioxide) was continuously determined by two non-dispersive infrared analysers connected in parallel (ABB EL3020 Caldos 27 and ABB EL3020 Uras26 with Magnos 206) Coke and water yields were calculated by closing carbon and hydrogen balances, respectively.

The rates of reaction, consumption of methane and product yields at any time during the reduction step over the different CLR experiments were calculated assuming; (i) the fix bed reactor is working at differential conditions (CH_4 conversion at any time during the reduction step is lower than 4%), (ii) transient (accumulation) effects can be ignored. Further information can be found in the supplementary information.

3. Results and discussion

3.1. Characterisation of mixed oxides of iron and cerium

The specific BET surface area for each oxide material are summarised in Table 1S and displayed in Fig. 1S (supplementary information). It can

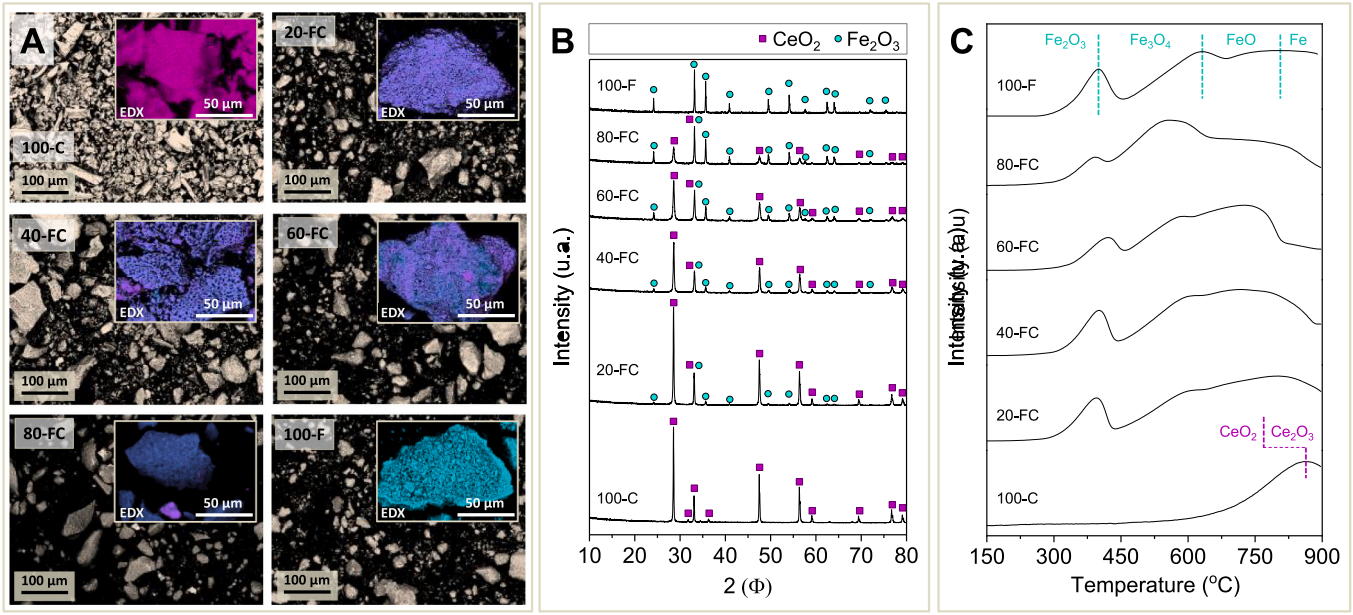

Fig. 1. Mixed oxides of iron and cerium after calcination for 1 h in air at 900 °C: A) SEM images and EDX surface mapping analysis, B) XRD patterns and C) Hydrogen TPR profiles.

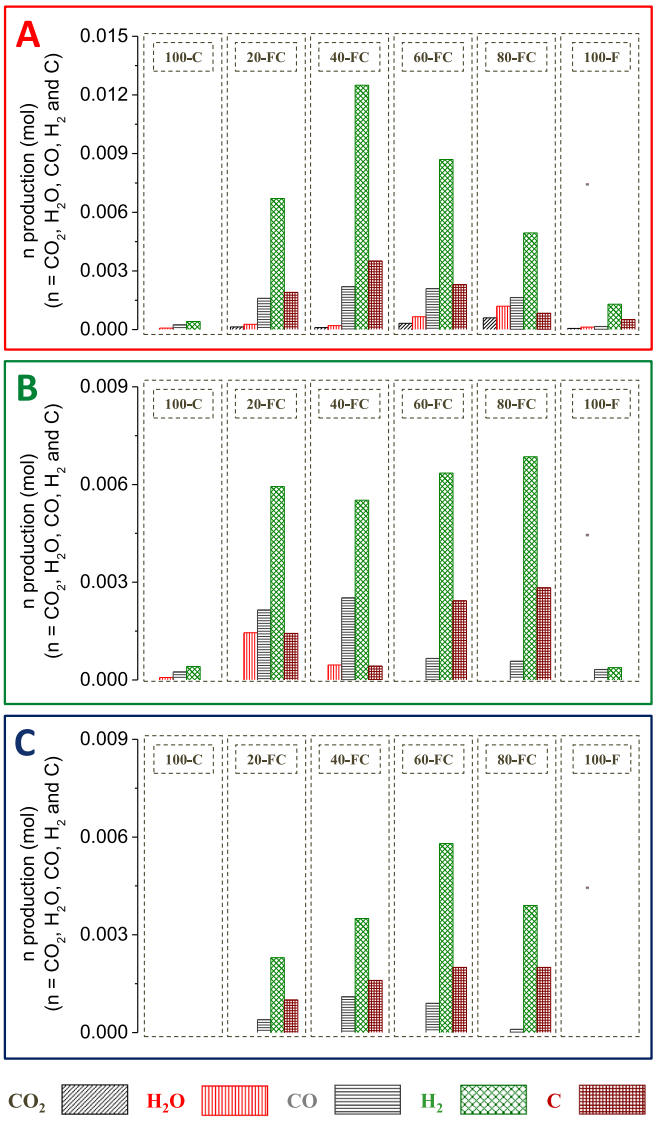

Fig. 2. Average of hydrogen, carbon monoxide, water, carbon dioxide and coke production over 10 CLR cycles using mixed oxides of iron and cerium. A) Activation in air (*i.e.* 90 min using 1.5 L/min (STP)), B) Activation in carbon dioxide (*i.e.* 90 min using 1.5 L/min (STP)), C) Activation in hydrogen (*i.e.* 90 min using 1.5 L/min (STP)).

be observed that mixed oxides of iron and cerium exhibit higher BET surface area than pure iron(III) and cerium(IV) oxides (except for the 20-FC mixed oxide). In this respect, it is worth stressing that the difference in the BET surface area is larger for those mixed oxides with lower cerium(IV) oxide content such as 60-FC and 80-FC mixed oxides. This behaviour could be tentatively explained by the structural promoter properties of the cerium oxide, which avoids the agglomeration of iron oxide crystallites during the calcination step.

The SEM images shown in Fig. 1 reflect that all mixed oxides of iron and cerium are crystalline materials. EDX mapping analysis suggests that at low iron(III) oxide loading (*i.e.*, samples 20-FC and 40-FC) iron and cerium oxides are homogenously mixture. However, at high iron(III) oxide loading (*i.e.*, samples 60-FC and 80-FC) small particles of cerium (IV) oxide are decorating the large iron(III) oxide crystallites.

Moreover, XRD results lead to the conclusion that, after calcination for 1 h at 900 °C in air, mixed oxides of iron and cerium are made up of two distinct phases: haematite (iron(III) oxide) and cubic fluorite (cerium(IV) oxide). The intensity of the haematite reflection peaks progressively decreased when the iron(III) oxide loading decreases (*i.e.*, haematite characteristic reflection peaks are 88% less intense in 20-FC than those observed in 100-F). This behaviour can be explained due to high dispersion of the iron(III) oxide particles on the cerium(IV) oxide at low iron(III) oxide loading (as observed in SEM photos).

Finally, Fig. 1D shows the crystallographic changes during the H_2-TPR for the different mixed oxides of iron and cerium. The H_2-TPR profile for pure Iron(III) oxide presents three peaks corresponding to the following transitions; (i) magnetite to haematite at 400 °C, (ii) haematite to wüstite at 636 °C, (iii) wüstite to metallic iron at 823 °C. However, the H_2-TPR profile of pure Cerium(IV) oxide only presents one peak corresponding with the transition from Cerium(IV) oxide to Cerium(III) oxide at 861 °C. The H_2-TPR profiles of pure Iron(III) oxide and pure Cerium(IV) oxide were used as a reference, hence the H_2-TPR profiles of the different mixed oxides of iron and cerium can be interpreted in terms of reduction of iron and cerium oxide phases.

3.2. Reaction experiments

In order to compare the reactivity of the different mixed oxides of iron and cerium, under the different activation atmospheres, 10 cycles' average hydrogen, carbon monoxide, water, carbon dioxide and coke yield normalized by the specific surface area are shown in Fig. 2. The evolution of hydrogen, carbon monoxide, water, carbon dioxide and coke rate profiles during the reduction step of each CLR experiment (*i.e.* activation in air, carbon dioxide and hydrogen) for the different mixed oxides of iron and cerium is shown in the supplementary information Fig. S2, S3, and S4.

It can be seem that in all CLR experiments hydrogen and carbon monoxide yields significantly increased when mixed oxides of iron and cerium are used compared to when pure iron and cerium oxides are used. This behaviour could be explained due to a synergetic interaction between both iron and cerium oxides. Among all samples, it was observed that 40-FC and 60-FC mixed oxides showed the highest activity, which is probably owing to the fine dispersion of iron oxide particles on the cerium oxide support. This not only results in an increase in the number of active sites, but also could favour the transfer of oxygen from the cerium(IV) oxide to the iron(III) oxide. Besides this, the formation of an iron-cerium mix oxide (*i.e.* $CeFeO_3$) could also explain the highest activity observed in these two samples. In this respect, Zhu et al. reported that mixed oxides of iron and cerium were transformed to $CeFeO_3$ *via* solid-solid reactions during the methane conversion step and that $CeFeO_3$ was reoxidised afterward to iron(III) oxide and cerium(IV) oxide during the regeneration step [7,8]. According to Zhu et al. oxygen mobility in mixed oxides of iron and cerium was intensified due to the formation of a perovskite type $CeFeO_3$. The formation of the $CeFeO_3$ was accompanied by a micromorphological transformation and the introduction of abundant oxygen vacancies, which promoted the high-temperature reducibility of the mixed oxide [7–9]. Likewise, Gu et all reported that after successive reduction/oxidation cycles the presence of cerium oxide also resulted in a significant improvement of the oxygen storage capacity of the mixed oxide compared to the single iron(III) oxide. The good reducibility of the $CeFeO_3$ suggested the potential of this material for redox process at high temperature such as chemical looping reforming [10]. Finally, Galvita et al. showed that the combination of both oxides efficiently suppressed the sintering, resulting in improved stability in chemical looping processes [11].

Fig. 2 also shows that the product selectivity observed in CLR experiments can be linked to a specific material oxidation state, which is fixed during the activation step and varies monotonically during the reaction time. For instance, production of carbon dioxide due to total oxidation of methane is only observed when materials have been activated in air. Likewise, carbon deposition *via* decomposition of methane over mixed oxides of iron and cerium occur at long reaction times when is likely to exist a substantial proportion of metallic iron present on their surface, see Fig. S2, and S3.

Fig. 3 shows a schematic diagram that attempts to illustrate the

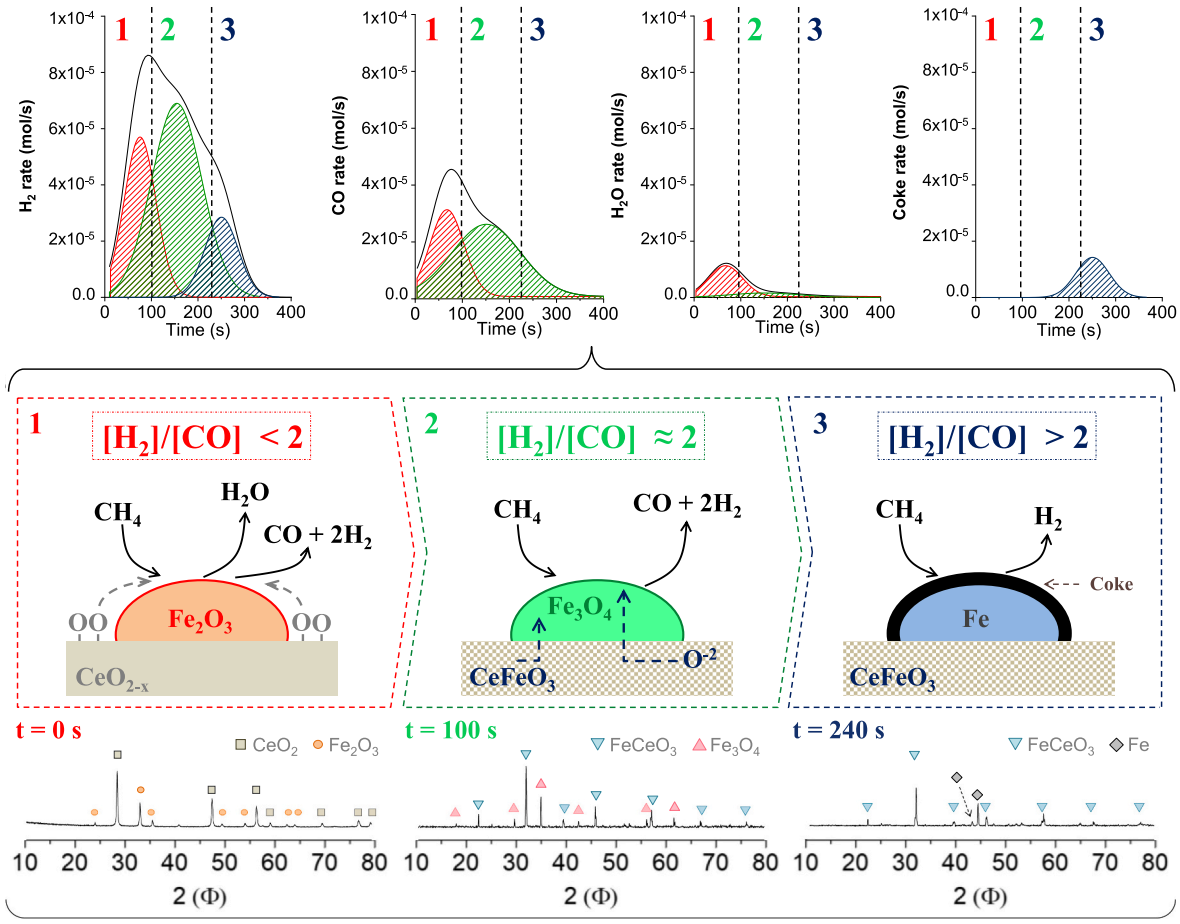

Fig. 3. Schematic diagram of the evolution and correlation between the product selectivity of 40-FC with its oxidation state during the reduction step of the CLR process after activation in carbon dioxide (*i.e.* 90 min using 1.5 L/min (STP)).

correlation between the product selectivity of 40-FC with its oxidation state. In order to avoid the total oxidation of methane, iron high oxidation states were avoided by activation in carbon dioxide. As can be seem, hydrogen production rate profile was deconvoluted into three subcomponents, whereas carbon monoxide and water production rate profiles were deconvoluted into two subcomponents. The $[H_2]/[CO]$ ratio at different reaction time intervals (*i.e.* 1, 2 and 3) was calculated by integration of the production rate *vs* time for each component and the oxidation state of 40-FC at the beginning of each reaction time interval was determined by *in-situ* XRD. This experiment shows that product selectivity and material oxidation state vary the reaction time in the following order: 1) oxidation of intermediate hydrogen species to water (high iron oxidation state), 2) partial oxidation of methane (intermediate iron oxidation state), and 3) decomposition of methane (low iron oxidation state).

In a similar way, Table 1 summarises the performance of mixed oxides of iron and cerium activated in carbon dioxide (evolution of hydrogen, carbon monoxide, water and coke rate profiles during the reduction step can be seem in Fig. 3S). It was observed that the $[H_2(a)]/[CO]$ ratio for materials with low iron(III) oxide content (*i.e.* $\leq$ 40 wt%) was lower than 2:1. This behaviour suggests that the intermediate hydrogen species produced during the activation of the C—H bond can be oxidised to form water. The formation of water during the early stages of the reduction step of the CLR process indicates the presence, initially, of very active oxygen in these materials. On the other hand, materials with large iron(III) oxide content (*i.e.* $\geq$ 40 wt%) showed higher $[H_2(b)]/[CO]$ ratio than those materials with a lower iron(III) oxide (*i.e.* $\leq$ 40 wt%) which can be explained due to the high decomposition of methane reaction rate in samples with large iron(III) oxide content.

Based upon the above, product selectivity of mixed oxides of iron and cerium during the CLR process can be adjusted by i) controlling their iron(III) oxide content, ii) selection of an adequate buffer gas during the activation step, and iii) limiting the duration of the reduction step of the CLR process. Therefore, it is possible to define an operation window, which could provide the best reactivity and product selectivity possible. Fig. 4 shows the iron-cerium phase diagram at reaction conditions employed during CLR experiments (*i.e.* $T = 900$ °C and $P = 1$ atm). In order to provide an overall picture of the product selectivity observed during different CLR experiments, its regions have been coloured: red for the total oxidation methane, green for the partial oxidation methane, blue for the decomposition of methane and white for the oxidation of intermediate hydrogen species to water. Based on this data, two different operation widows for CLR have been identified. Materials with large iron(III) oxide content (*i.e.* $\geq$ 50 wt%) can be cycled in the Log pO_2 range from −5 to −12 (*i.e.* operation window 1). Whereas, materials with medium iron(III) oxide content (*i.e.* from 20 wt% to 50 wt%) have to be cycled in the Log pO_2 range from −10 to −15 (*i.e.* operation window 2).

4. Conclusions

The hydrogen and carbon monoxide yields for both iron(III) and cerium(IV) oxides during the reduction step of different CLR experiments is much lower than that observed for the different mixed oxides of iron and cerium. The higher hydrogen and carbon monoxide yields observed over mixed oxides of iron and cerium could be explained due; (i) synergetic interaction between both iron and cerium oxides, (ii) fine

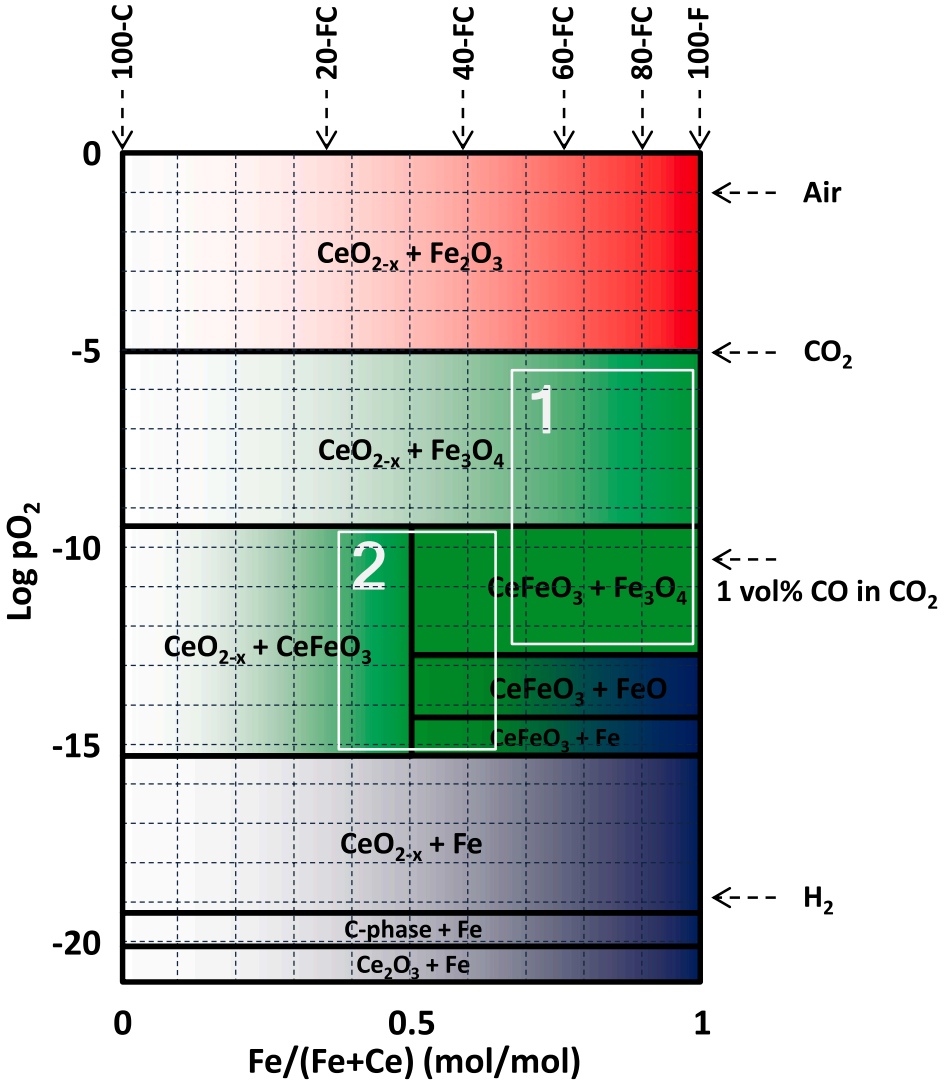

Fig. 4. Iron-cerium phase diagram shows which phases and product selectivity during the reduction step of the CRM process of are to be expected at equilibrium for different combinations of iron-cerium content and oxygen chemical potential at $T = 900$ °C and $P = 1$ atm.

dispersion of iron oxide particles on the cerium oxide support, (iii) formation of a peruskite type oxide (*i.e.* $CeFeO_3$).

The product selectivity of the different mixed oxides of iron and cerium during the reduction step of the CLR can be adjusted by controlling their iron(III) oxide content. For example, materials with large iron(III) oxide content (*i.e.*, $\geq$ 40 wt%) showed higher coke yield than those materials with a lower iron(III) oxide (*i.e.*, $\leq$ 40 wt%) which can be explained due to the high decomposition of methane reaction rate in samples with large iron(III) oxide content. Likewise, intermediate hydrogen species produced during the activation of the C—H bond can be oxidised to water in materials with lower iron(III) oxide content (*i.e.*, $\geq$ 40 wt%).

Finally, the product selectivity during the CL-DRM can be linked to a specific material oxidation state which is fixed during the activation step and varies monotonically during the reaction time. Hence, in order to avoid the total oxidation of methane, high oxidation states can be avoided by activation in carbon dioxide. Whereas, low iron oxidation states can be circumvented by limiting the duration of the reduction step of the CL-DRM process, in an attempt to overcome carbon deposition.

Credit author statement

F.R. García–García: Methodology, Experimental work, Investigation (lead), Writing – Original draft preparation (lead), Writing - Review & Editing (lead).

I.S. Metcalfe: Resources, Supervision, Investigation (supporting), Writing – Original draft preparation (supporting), Writing - Review & Editing (supporting).

Declaration of Competing Interest

The authors declare that they have no known competing financial interests or personal relationships that could have appeared to influence the work reported in this paper.

Acknowledgements

This work was supported by the funding provided by EPSRC in the UK (EP/K014706/2).

Appendix A. Supplementary data

Supplementary data to this article can be found online at https://doi.org/10.1016/j.catcom.2021.106356.

References

[1] J. Adánez, A. Abad, F. García-Labiano, P. Gayán, L.F. De Diego, Progress in chemical-looping combustion and reforming technologies, Prog. Energ. Combust. 38 (2012) 215–282.
[2] L. Kongzhai, W. Hua, W. Yonggang, L. Mingchun, Catalytic performance of cerium iron complex oxides for partial oxidation of methane to synthesis gas, J. Rare Earths 26 (2008) 705–710.
[3] W. Yonggang, W. Hua, L. Kongzhai, Ce-Fe-O mixed oxide as oxygen carrier for the direct partial oxidation of methane to syngas, J. Rare Earths 28 (2010) 560–565.
[4] L. Kongzhai, W. Hua, W. Yonggang, L. Mingchun, Preparation and characterization of Ce1-xFexO2 complex oxides and its catalytic activity for methane selective oxidation, J. Rare Earths 26 (2008) 245–249.
[5] K. Watanabe, T. Miyao, K. Higashiyama, H. Yamashita, M. Watanabe, Preparation of a mesoporous ceria–zirconia supported Ni–Fe catalyst for the high temperature water–gas shift reaction, Catal. Commun. 12 (2011) 976–986.
[6] S. Brunauer, L.S. Deming, W.E. Deming, E. Teller, On a theory of the van der Waals adsorption of gases, J. Am. Chem. Soc. 62 (1940) 1723–1732.
[7] M. Kakihana, "Sol-Gel" preparation of high temperature superconducting oxides, J. Sol-Gel Sci. Technol. 6 (1996), 7–55.V.
[8] Y. Wu, X. Wang, Preparation and characterization of single-phase α-Fe_2O_3nano-powders by Pechini sol–gel method, Mater. Lett. 65 (2011) 2062–2065.
[9] B. Secerov, Z. Andric, N. Abazovic, R. Krsmanovic, M. Mitric, A. Montone, M. D. Dramicanin, Combustion synthesis and characterization of CeO2 Nanopowder, Acta Chim. Slov. 55 (2008) 486–491.
[10] G.S. Li, R.L. Smith, H. Inomata, Synthesis of nanoscale Ce1-xFexO2 solid solutions via a low-temperature approach, J. Am. Chem. Soc. 123 (2001) 11091–11092.
[11] F.J. Perez-Alonso, I. Melián-Cabrera, M. López Granados, F. Kapteijn, J.L.G. Fierro, Synergy of FexCe1−xO2 mixed oxides for N2O decomposition, J. Catal. 239 (2006) 340–346.